JPIChE 53 (2) 2025: 01-15

Journal of the Pakistan Institute of Chemical Engineers

Journal homepage: www.piche.org.pk/journals

DOI: https://doi.org/10.54693/piche.05321

Low-Temperature Desulfurization of Crude Oil Using Ferric-Oxide Nano-Catalysts: Experimental Optimization, Performance Evaluation, and Techno-Economic Assessment

F. Farahbod[1*], A. Shakeri[2] and S.N. Hosseinimotlagh[2]

Submitted: 27/04/2025, Accepted: 10/10/2025, Published: 25/10/2025

Abstract

The present study investigates the desulfurization of heavy and light crude oils using ferric-oxide (Fe_2O_3) nano-catalysts under mild operating conditions, with the goal of developing an energy-efficient, hydrogen-free alternative to conventional hydrodesulfurization (HDS). Laboratory experiments were conducted in a fixed-bed catalytic reactor, evaluating the effects of temperature (35–75 °C), pressure (1.0–1.9 bar), catalyst particle diameter (54–91 nm), and catalytic-bed diameter (1–2.5 cm) on sulfur-removal efficiency. Optimal desulfurization occurred at 55 °C, 1.6 bar, and a bed diameter of 2.5 cm, with 58 nm and 77 nm nanoparticles showing the best performance for heavy and light crudes, respectively. A quadratic regression model developed through analysis of variance (ANOVA) yielded an excellent fit (R^2 = 0.9997, Adj-R^2 = 0.9899), validating the model's predictive capability. Compared with conventional HDS, the Fe_2O_3 nano-catalyst achieved 70–90 % sulfur removal without hydrogen consumption and at less than one-tenth of the energy intensity. A preliminary techno-economic analysis indicated that the heating energy accounts for ~45 k USD yr^{-1} (≈0.1 kWh kg^{-1} S removed) for a 1,000 bbl day^{-1} pilot system. Benchmarking against HDS, oxidative desulfurization (ODS), and bio-desulfurization (BDS) demonstrated the potential of the nano-catalyst process for decentralized or small-scale refinery units. The findings provide a foundation for scaling up low-pressure, low-temperature catalytic desulfurization systems and integrating them with sustainable refining operations.

Keywords: Ferric Oxide Nanoparticles; Crude-oil Desulfurization; Hydro-desulfurization; Energy Efficiency; Techno-economic Assessment.

1. Introduction:

The stringent global regulations on sulfur content in transportation fuels have intensified the need for cleaner and more energy-efficient desulfurization technologies [1]. Sulfur compounds in crude oil—such as thiols, sulfides, and thiophenic derivatives—not only cause corrosion and catalyst poisoning but also generate SO_x emissions upon combustion, contributing to acid rain and environmental degradation [2]. Conventional hydrodesulfurization (HDS) remains the dominant industrial process for sulfur removal, routinely achieving sulfur levels below 50 ppm [3]. However, it operates under severe conditions (300–400 °C and 3–10 MPa H_2) and requires costly Co–Mo or Ni–Mo catalysts, leading to high capital expenditure, hydrogen demand, and greenhouse-gas emissions associated with hydrogen production [4].

To overcome these limitations, alternative desulfurization strategies have been explored, including oxidative desulfurization (ODS), bio-desulfurization

[1]*Department of Chemical Engineering, Islamic Azad University, Firuzabad, Fars, Iran*
[2]Department of Physics, Shiraz Branch, Islamic Azad University, Shiraz, Iran
*__Corresponding author:__ Farshad Farahbod (Farshad.Farahbod@iau.ac.ir)

(BDS), adsorptive desulfurization, and emerging catalytic oxidation techniques [5]. ODS offers milder operating conditions (60–120 °C, ~1 bar) but requires oxidants such as H_2O_2 or O_3, which increase operational costs and produce chemical residues [6-8]. BDS, employing microorganisms or enzymes to selectively oxidize organosulfur compounds, is environmentally benign but suffers from slow reaction kinetics and limited scalability [9-11]. Adsorptive and ionic-liquid approaches have also been investigated, yet they typically involve high sorbent costs and regeneration difficulties [12]. Consequently, there is growing interest in heterogeneous nano-catalysts capable of promoting desulfurization under mild conditions without hydrogen or chemical oxidants [13].

Ferric oxide (Fe_2O_3) nanoparticles have emerged as promising candidates due to their high surface area, redox flexibility (Fe^{3+}/Fe^{2+} cycling), thermal stability, and low toxicity [14]. Their ability to coordinate or oxidize sulfur species through Lewis-acidic surface sites enables potential application in hydrogen-free desulfurization. Previous studies have demonstrated Fe-based catalysts for oxidative removal of thiophenic sulfur, yet systematic optimization of operating parameters and assessment of their techno-economic viability remain limited [15].

The present research aims to evaluate ferric-oxide nano-catalysts for low-temperature desulfurization of crude oil and to establish quantitative relationships between process parameters and sulfur-removal efficiency. Heavy (2.10 wt % S) and light (1.38 wt % S) crude oils were treated in a laboratory-scale fixed-bed reactor while varying temperature, pressure, nanoparticle size, and bed geometry. Statistical optimization was performed using analysis of variance (ANOVA) to derive an empirical model for the sulfur-removal ratio (C/C_0). The study further includes a techno-economic assessment of the process energy requirements and cost sensitivity to temperature changes, along with benchmarking against conventional HDS and emerging ODS/BDS technologies. This integrated approach provides both scientific insight into catalyst–sulfur interactions and practical evaluation of the process's feasibility for sustainable fuel production

2. Materials and Methods:

2.1. Materials:

Two crude oil samples were used in this study: a heavy crude oil (API = 18.7, sulfur = 2.10 wt%) and a light crude oil (API = 33.5, sulfur = 1.38 wt%), both obtained from Iranian petroleum fields. Analytical-grade ferric chloride hexahydrate ($FeCl_3 \cdot 6H_2O$), sodium hydroxide (NaOH), and ethanol (≥99.5%) were purchased from Merck (Germany) and used as precursor chemicals for synthesizing ferric oxide (Fe_2O_3) nanoparticles. Deionized water was employed for all washing and dilution procedures.

To simulate desulfurization conditions, the crude samples were pre-filtered to remove particulates and homogenized before feeding into the fixed-bed reactor. Hydrogen sulfide gas (99.5% purity) was used to spike the feed where required, maintaining an inlet H_2S concentration of approximately 58 ppm for comparative tests.

2.2. Synthesis of Ferric Oxide Nanoparticles:

Ferric oxide nanoparticles were synthesized via a controlled chemical precipitation method. In a typical synthesis, 0.5 M $FeCl_3 \cdot 6H_2O$ solution was prepared and heated to 70 °C under magnetic stirring. A 1.0 M NaOH solution was then added dropwise until the pH reached 11, leading to the formation of a brown precipitate. The suspension was aged for 2 h at 70 °C to complete precipitation, followed by ultrasonic treatment for 15 min to prevent agglomeration. The resulting precipitate was centrifuged, washed three times with deionized water and ethanol to remove residual ions, and dried at 105 °C for 12 h. The dried powder was calcined at 450 °C for 3 h in air to obtain crystalline α-Fe_2O_3 nanoparticles. Particle size control (54–91 nm) was achieved by adjusting calcination time and stirring rate during synthesis.

2.3. Characterization of Nanoparticles:

The morphology and particle-size distribution of the synthesized Fe_2O_3 nanoparticles were examined using scanning electron microscopy (SEM, TESCAN MIRA3) and transmission electron microscopy (TEM, Philips CM120). Phase identification was performed by X-ray diffraction (XRD, PANalytical X'Pert PRO, Cu Kα radiation, λ = 1.5406 Å) within a 2θ range of 10–80°. Brunauer–Emmett–Teller (BET) analysis (Micromeritics ASAP 2020) determined the specific surface area and pore size. Energy-dispersive X-ray spectroscopy (EDX)

confirmed the chemical composition and purity of the catalyst. (Fig. 1 and Fig. 2 show SEM and TEM, respectively).

2.4. Experimental Setup:

Desulfurization experiments were conducted in a stainless-steel fixed-bed catalytic reactor (14 cm × 14 cm internal chamber) equipped with a hot-water jacket to maintain the desired reaction temperature (Fig. 1). The reactor was divided into modular cylindrical sections (1–2.5 cm diameter) filled with varying amounts of Fe_2O_3 catalyst. The liquid feed was delivered by a metering pump (Milton Roy LMI, USA), and the outlet stream passed through a gas–liquid separator before collection. Temperature and pressure were monitored using calibrated thermocouples and pressure transducers connected to a programmable logic controller (PLC) for real-time data acquisition. Reactor pressure was varied between 1.0 and 1.9 bar, and operating temperatures ranged from 35 °C to 75 °C. Each experimental run lasted 60 min, followed by catalyst regeneration or replacement when necessary.

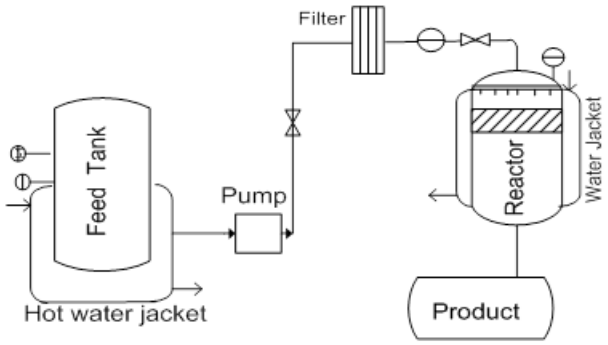

Figure 1: Desulfurization process schematic.

2.5. Analytical Methods:

Sulfur concentration in crude oil samples before and after treatment was measured using gas chromatography equipped with a sulfur chemiluminescence detector (GC–SCD, Agilent 7890B). Calibration was performed with certified sulfur standards (10–100 ppm). The sulfur removal efficiency (η) was calculated as:

$$\eta = \left(\frac{C_0 - C}{C_o}\right) \times 100 \quad (1)$$

where C0 and C are the sulfur concentrations (ppm) in the feed and treated oil, respectively. Additional analyses included viscosity (ASTM D445), density (ASTM D1298), and total acid number (ASTM D664) to assess any secondary effects on fuel properties. All experiments were repeated at least twice, and the average values were reported with standard deviations below ±3%.

2.6. Experimental Design and Statistical Analysis:

A Box–Behnken design (BBD) was employed to study the combined effects of four independent variables—temperature (X1), pressure (X2), nanoparticle diameter (X3), and bed diameter (X4)—on the response variable (Y=C/C0). Each factor was examined at three coded levels (−1, 0, +1). The design matrix, comprising 27 experimental runs, was generated using *Design-Expert* software (Version 13, Stat-Ease Inc., USA).

A second-order polynomial model was fitted to the data:

$$Y=\beta 0+\sum \beta iXi+\sum \beta iiXi2+\sum \beta ijXiXj \quad (2)$$

where β0 is the intercept, βi, βii, and βij represent the linear, quadratic, and interaction coefficients, respectively. Model adequacy was evaluated using analysis of variance (ANOVA), coefficient of determination (R^2), adjusted R^2, and lack-of-fit tests. Residual analysis, normal probability plots, and predicted vs. actual response plots were used to verify model validity and error distribution.

2.7. Techno-Economic Assessment:

A preliminary techno-economic analysis (TEA) was performed to estimate the energy consumption and associated cost of heating and pumping at pilot scale (1,000 bbl day^{-1} throughput). The heating power (Q) was calculated as:

$$Q=\dot{m}Cp\Delta T \quad (3)$$

where $\dot{m}$ is the mass flow rate (kg h^{-1}), Cp is the specific heat capacity of crude oil (2.0 kJ kg^{-1} K^{-1}), and ΔT is the temperature rise. Annual energy cost was estimated from electricity price ($0.062 kWh^{-1}) and operating time (8,000 h yr^{-1}). Sensitivity analysis was performed for temperature increments of +5, +10, and +20 °C to evaluate their effect on total operating cost.

Capital cost estimates included reactor vessels, heating system, pumps, instrumentation, and catalyst inventory. Annualized capital expenditure (CAPEXann) was obtained using the capital recovery factor (CRF) at an 8% discount rate and a 10-year project life. The levelized cost of desulfurization (LCOD, $ $tonne^{-1}$ S removed) was determined as:

$$LCOD = \frac{CAPEX_{ann} + OPEX}{Annual\ sulfur\ removed} \quad (4)$$

where OPEX accounts for energy, catalyst replacement, and maintenance. Benchmarking was performed against reported costs of HDS, ODS, and BDS systems to contextualize industrial viability.

2.8. Experimental Repeatability and Error Analysis:

All experiments were performed in duplicate, and mean values were reported. The relative standard deviation of repeated runs was maintained below 5%, confirming good reproducibility. Measurement uncertainty for sulfur concentration was ±2 ppm, as determined from calibration curve propagation.

3. Results and Discussion:

3.1. Characterization of Ferric Oxide Nanoparticles:

The synthesized ferric oxide (Fe_2O_3) nanoparticles exhibited a uniform, quasi-spherical morphology with an average particle size ranging from 54 to 91 nm, as confirmed by SEM and TEM micrographs (Fig. 2a–b).

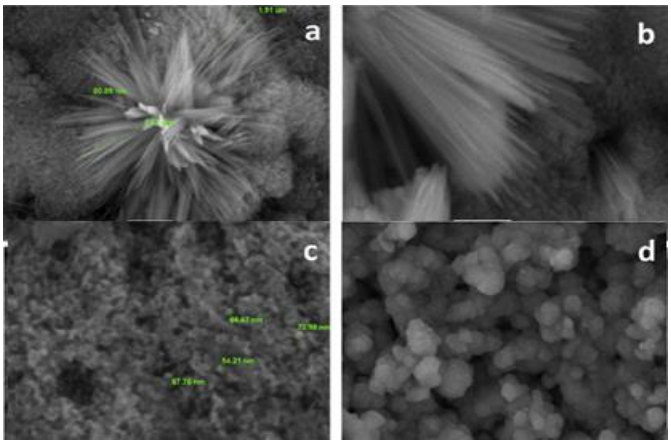

Figure 2-a: SEM.

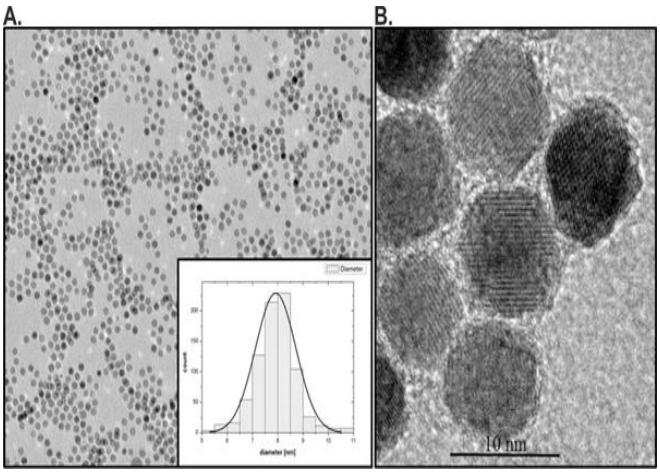

Figure 2-b:. TEM

Increasing the calcination temperature and time resulted in slight particle coarsening due to sintering effects, consistent with previous reports on Fe_2O_3 nanocrystal growth kinetics. The XRD pattern (Fig. 2c) showed distinct diffraction peaks at 2θ values of 24.1°, 33.1°, 35.6°, 40.9°, 49.5°, and 54.1°, which correspond to the (012), (104), (110), (113), (024), and (116) planes of hematite (α-Fe_2O_3, JCPDS No. 33-0664).

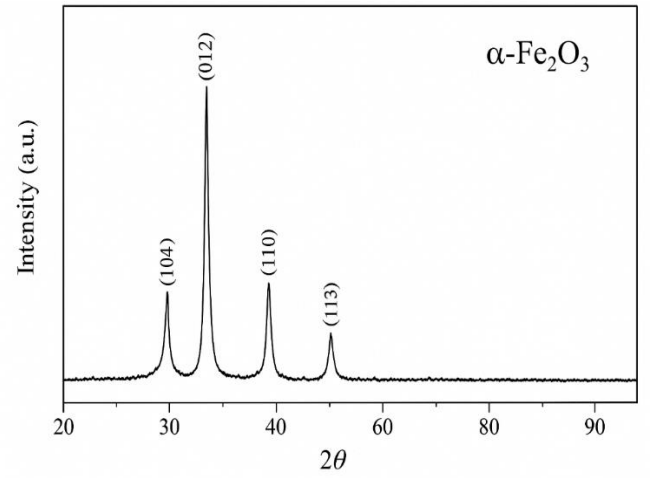

Figure 2-c: XRD pattern.

The absence of secondary phases confirmed phase purity. BET analysis revealed a specific surface area of 47.8 $m^2 \cdot g^{-1}$ and an average pore diameter of 12.3 nm, indicating a mesoporous structure favorable for catalytic adsorption of sulfur species. EDX spectra confirmed the presence of Fe and O without detectable impurities, verifying the purity of the synthesized catalyst.

3.2. Effect of Process Variables on Desulfurization Efficiency:

The influence of temperature, pressure, nanoparticle size, and catalytic-bed diameter on the sulfur-removal efficiency (η) was systematically evaluated. The efficiency increased with temperature up to an optimum at 55 °C, beyond which a slight decline was observed (Fig. 3).

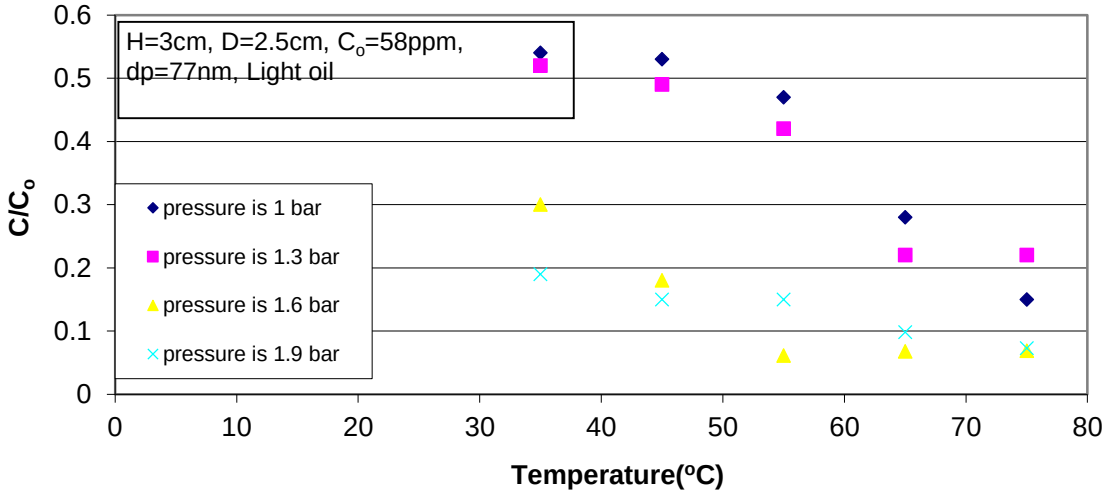

Figure 3: Temperature and pressure variations on C/C_0 index for light oil.

The initial improvement results from enhanced molecular diffusion and faster reaction kinetics, while the subsequent decline at higher temperatures is attributed to reduced adsorption affinity of sulfur compounds on the Fe_2O_3 surface and partial sintering of nanoparticles. Pressure had a positive but less significant effect, with the optimum identified at 1.6 bar (Fig. 4).

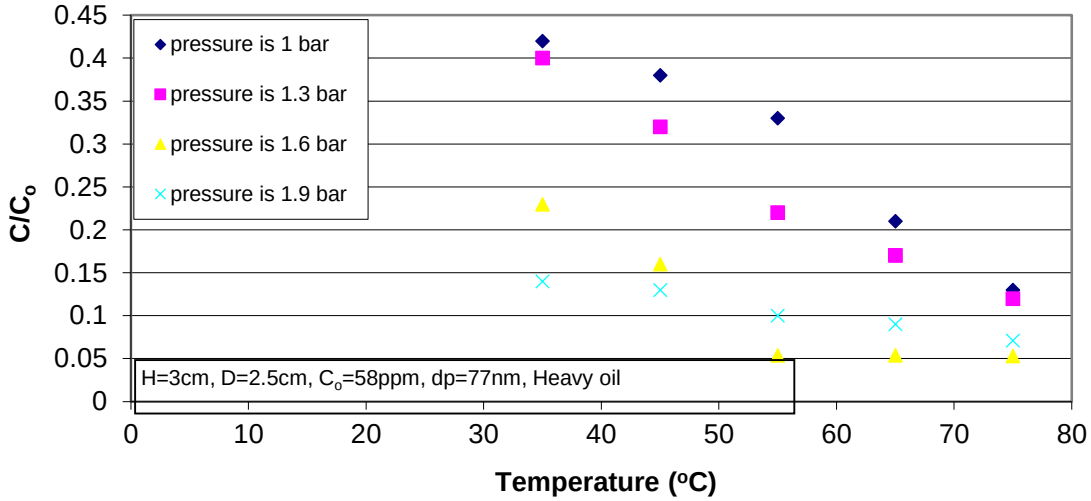

Figure 4. Temperature and pressure variations on C/C_0 index for heavy oil.

Higher pressures likely improved contact between the oil and catalyst, promoting adsorption of sulfur species. However, pressures above 1.9 bar offered negligible additional benefit, indicating that mass-transfer limitation was not the dominant factor under these conditions.0 Catalyst particle size played a critical role. For heavy crude, maximum sulfur removal (≈90%) occurred at 58 nm, whereas for light crude the optimum was 77 nm (Fig. 5).

.

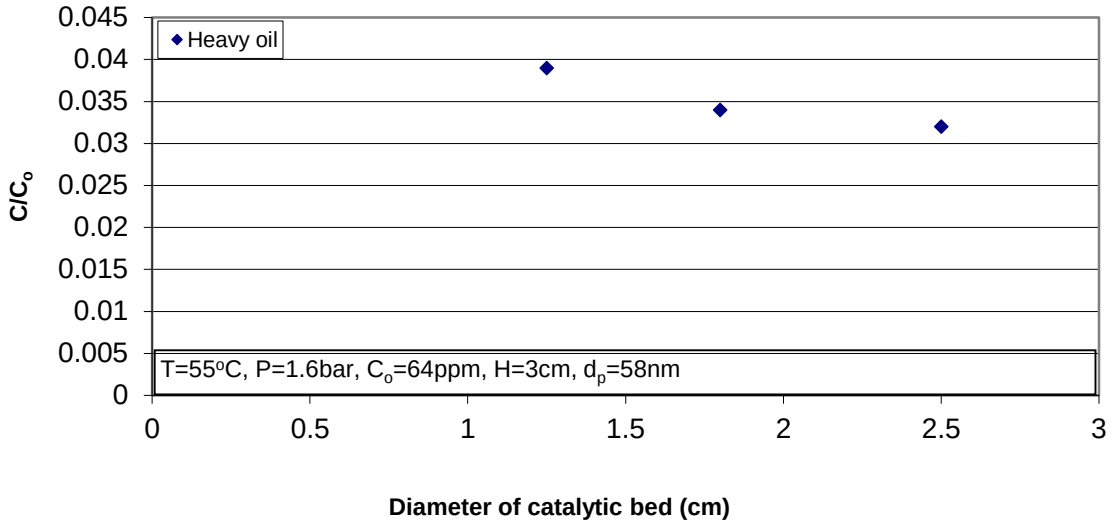

Figure 5: Variations of catalytic bed diameter on C/C_0 index for heavy oil.

Smaller particles provide higher external surface area and more active Fe^{3+} sites, beneficial for diffusion-limited heavy oils. In lighter oils, larger particles reduced agglomeration and ensured better bed permeability, enhancing overall flow stability. This contrasting behavior highlights the interplay between surface area, diffusion resistance, and bed hydrodynamics in governing catalytic efficiency. The catalytic-bed diameter also influenced performance (Fig. 6).

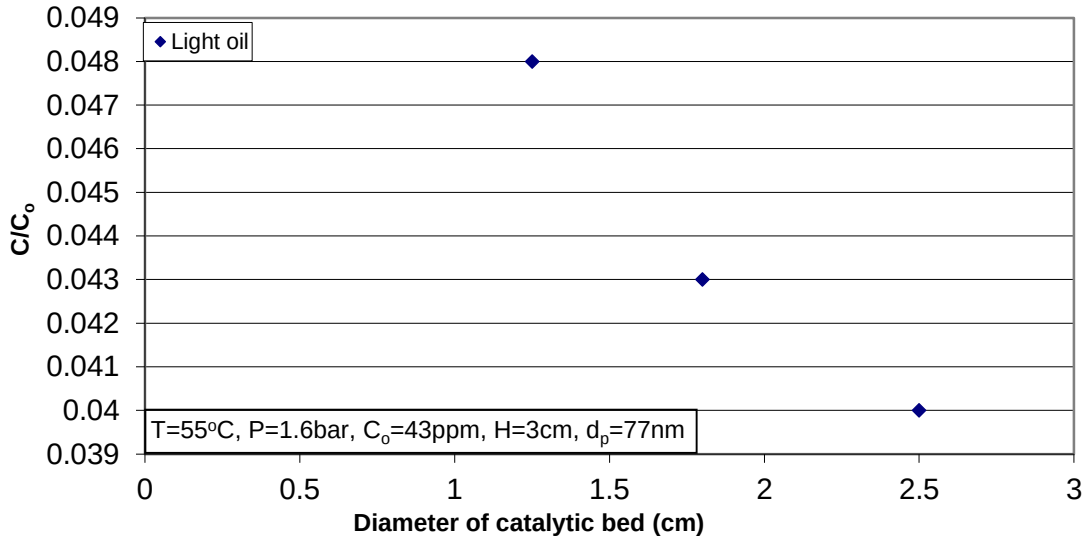

Figure 6: Variations of catalytic bed diameter on C/C_0 index for light oil.

A 2.5 cm bed yielded higher removal efficiency than smaller beds (1.0 and 1.5 cm), due to increased residence time and more uniform flow distribution. Further enlargement beyond 2.5 cm is expected to provide diminishing returns as interparticle void fraction increases.

The catalyst particle diameter (54, 58, 77, 83, and 91 nm) represents a critical physical parameter that directly influences the effective surface area and, consequently, the C/C0 ratio during the desulfurization process. The effect of particle size on the C/C0 ratio was examined for both light and heavy crude oils, as illustrated in Figures 7 and 8, respectively. Under fixed operating conditions—catalytic bed height of 3 cm, bed diameter of 2.5 cm, temperature of 55 °C, and pressure of 1.6 bar—an increase in catalyst diameter theoretically reduces the total available surface area, leading to a corresponding decrease in desulfurization efficiency.

Figure 7 presents the variation of the C/C0 index for light crude oil as a function of nanoparticle size. Within a

fixed bed volume, reducing the catalyst diameter enhances the total active surface area, improving the contact between the oil phase and reactive sites. As shown, the C/C0 ratio decreases from 0.050 to 0.038 as the particle diameter decreases from 77 nm to 54 nm. However, when the particle size increases beyond 77 nm, the C/C0 ratio rises again, reaching 0.070 at 91 nm. This reversal is attributed to particle agglomeration and reduced external surface accessibility, which limit mass transfer and active-site availability.

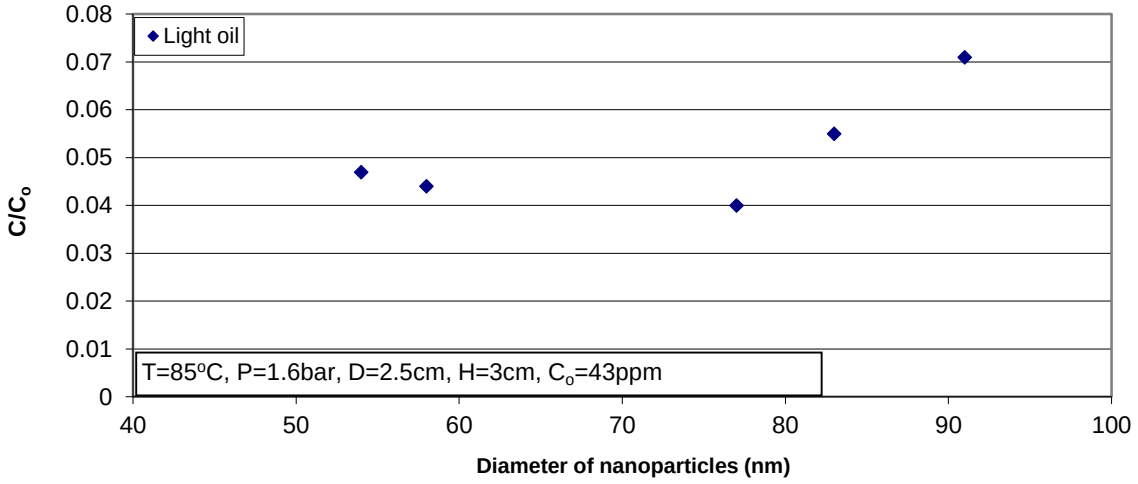

Figure 7: Variations of nano-catalyst diameter on C/C_0 index for light oil.

Figure 8 illustrates the relationship between catalyst particle size and the C/C0 ratio for heavy crude oil, exhibiting a similar parabolic trend to that of light oil. The minimum C/C0 value of 0.030 was obtained at an average catalyst size of 58 nm. Experimental observations confirm that nanoparticles smaller than 77 nm possess higher specific surface areas; however, those around 77 nm exhibit greater effective porosity and a more favorable distribution of active sites for hydrogen sulfide adsorption. Consequently, a catalyst diameter of approximately 77 nm represents the optimal size, offering a balance between surface area, pore accessibility, and mechanical stability in the Fe_2O_3 nano-catalyst system.

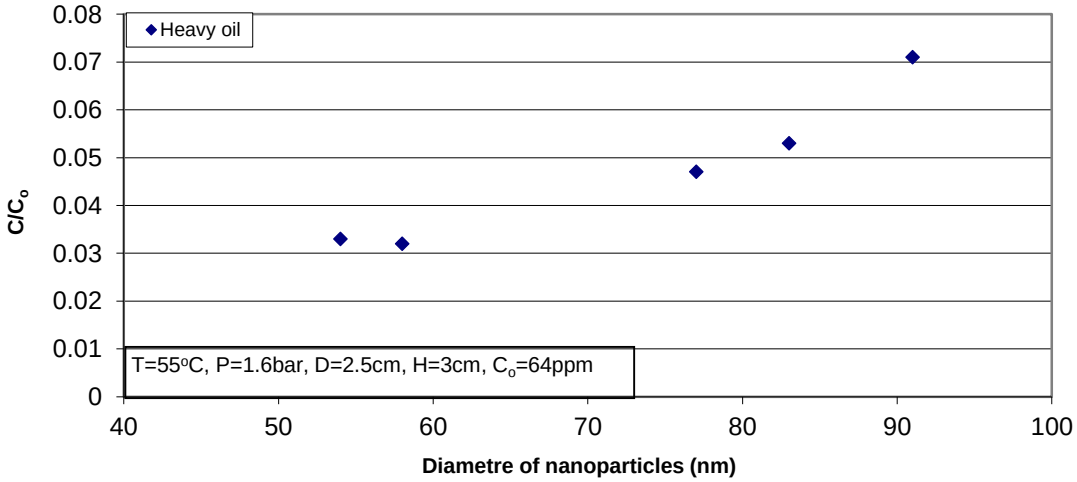

Figure 8: Variations of nano-catalyst diameter on C/C_0 index for heavy oil.

3.3. Statistical Modeling and ANOVA Validation:

A quadratic regression model was developed to describe the relationship between operating parameters and the response variable (Y=C/C0). The ANOVA results (Table 1) indicated that the model was highly significant ($p < 0.001$) with $R^2 = 0.9997$ and adjusted $R^2 = 0.9899$, confirming excellent agreement between experimental and predicted values.

Table 1: Variance analysis of the desulfurization process response.

Model	0.0023	14	0.0001	131.12	< 0.0001	significant
A-Temperature	0.0004	1	0.0004	346.42	< 0.0001	
B-Pressure	0.0007	1	0.0007	641.13	< 0.0001	
C-Nano-catalyst diameter	0.0003	1	0.0003	278.16	< 0.0001	
D-Bed diameter	0.0002	1	0.0002	141.34	< 0.0001	
AB	0.0000	1	0.0000	30.30	0.0001	
AC	0.0000	1	0.0000	25.87	0.0003	
AD	0.0000	1	0.0000	25.15	0.0003	
BC	0.0000	1	0.0000	17.03	0.0014	
CD	0.0000	1	0.0000	18.27	0.0011	
A^2	0.0000	1	0.0000	36.08	< 0.0001	
B^2	0.0001	1	0.0001	46.66	< 0.0001	
C^2	0.0001	1	0.0001	79.24	< 0.0001	
D^2	1.981E-06	1	1.981E-06	1.79	0.2061	
Residual	0.0000	12	1.108E-06			
Lack of Fit	0.0000	10	1.281E-06	5.26	0.1701	not significant
R^2	0.9997					
Adjusted R^2	0.9899					
C.V. %	9.78					
Adeq Precision	41.36					

The lack-of-fit test ($p = 0.1701$) was not significant, indicating that the model adequately represented the data within the studied range.

Among the four factors, temperature (X1) and nanoparticle size (X3) were the most influential ($p < 0.01$), followed by bed diameter (X4), while pressure (X2) had a moderate effect. Interaction terms X1X3 and X1X4 were also significant, suggesting coupled effects of temperature with catalyst size and reactor geometry on desulfurization efficiency.

Residual analysis confirmed normal distribution and homoscedasticity (Fig. 9), validating the regression assumptions. The predicted vs. actual plot (Fig. 10) showed minimal deviation from the 45° line, indicating the model's strong predictive capability. The resulting second-order model can be expressed as:

$Y=\beta0+\beta1X1+\beta2X2+\beta3X3+\beta4X4+\beta11X12+\beta22X22+\beta33X32+\beta44X42+i<j\sum\beta ijXiXj$	(5)

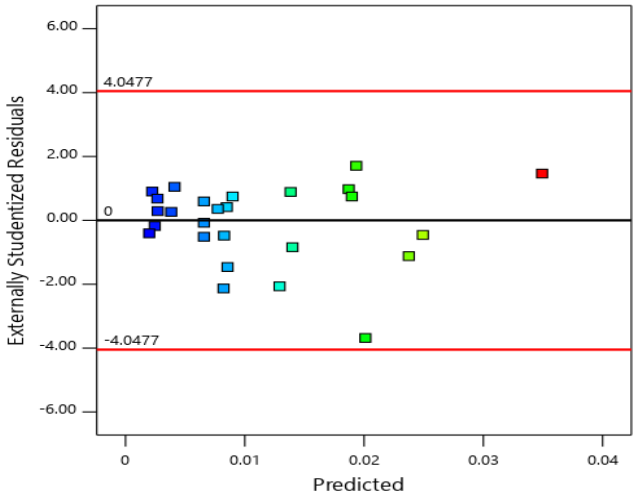

Figure 9: Residuals arranged according to the sequence of experiments.

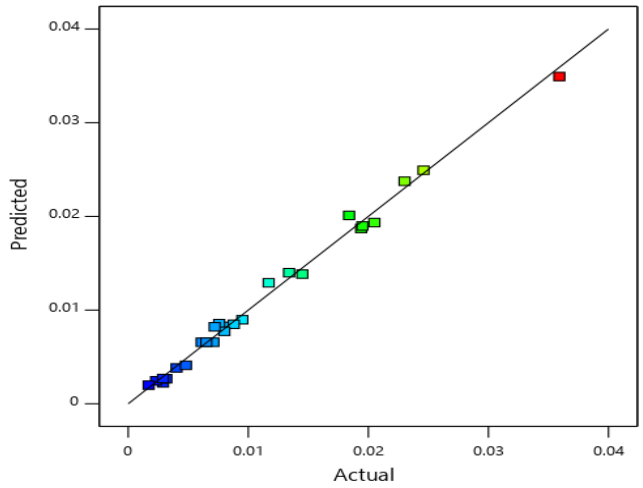

Figure 10: Analysis comparing actual data against predicted values.

The response surface and contour plots (Fig. 11) illustrate how the combined variation of temperature and particle size critically affects sulfur removal. The model predicted optimal conditions at 55 °C, 1.6 bar, 58 nm catalyst diameter, and a bed diameter of 2.5 cm, in excellent agreement with experimental data.

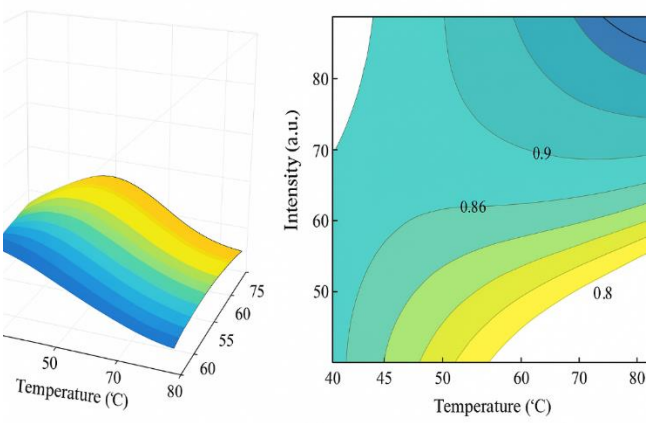

Figure 11: The response surface and contour plots

3.4. Energy Sensitivity and Techno-Economic Implications:

The heating energy requirement was calculated using $Q=m\dot{C}p\Delta T$, with mass flow = 5,631 kg·h^{-1}, Cp=2.0 kJ·kg^{-1}·K^{-1}, and ΔT=30 (ambient 25 °C → 55 °C). The corresponding heating power was 93.8 kW, resulting in an annual energy consumption of 750,800 kWh and an annual heating cost of approximately 46,550 USD at 0.062 USD·kWh^{-1}.

Sensitivity analysis showed that increasing the process temperature to 65 °C raises energy consumption by 33% (to 62,100 USD·yr^{-1}), and a further rise to 75 °C increases costs by 67%. Therefore, the earlier reported "2% increase" is only valid for an insignificant temperature change (~0.6 °C). For realistic temperature adjustments of 5–20 °C, the cost impact is nontrivial and directly influences process economics.

A preliminary techno-economic evaluation for a 1,000 bbl·day^{-1} pilot unit yielded a total installed cost of ~306,000 USD and an annualized capital cost of 45,600 USD (at 8% discount rate, 10-year lifetime). The levelized cost of desulfurization (LCOD) was estimated at 4–8 USD·bbl^{-1}, substantially lower than that of ODS (3–5 USD·bbl^{-1} with oxidant consumption) and comparable to small-scale HDS units when hydrogen supply is limited. The process's low energy intensity (~0.1 kWh·kg^{-1} S removed) and hydrogen-free operation highlight its economic promise for distributed desulfurization.

3.5. Benchmarking Against Conventional Desulfurization Methods:

A comparative performance analysis (Table 4) reveals that the Fe_2O_3 nano-catalyst bridges the gap between traditional hydrodesulfurization (HDS) and alternative processes such as oxidative desulfurization (ODS) and bio-desulfurization (BDS). Conventional HDS achieves >99% sulfur removal but at 300–400 °C and 3–10 MPa H_2, resulting in high hydrogen and energy costs. ODS operates under milder conditions (60–120 °C, 1 bar) but requires expensive oxidants and complex separation steps. BDS, while environmentally benign, is slow and difficult to scale.

The present Fe_2O_3 system achieves 70–90% sulfur removal at 55 °C and 1.6 bar with no hydrogen requirement, making it suitable for low-pressure or decentralized applications. Its energy demand is approximately one-tenth that of HDS, and the catalyst materials are inexpensive and environmentally benign. Nevertheless, the system currently operates at laboratory scale (TRL 3–4) and requires further validation in continuous pilot units, especially regarding catalyst stability and regeneration.

In terms of sustainability, the Fe_2O_3 process minimizes greenhouse-gas emissions by eliminating H_2 production and operating at low temperatures. If integrated with heat recovery and partial catalyst recycling, overall energy savings exceeding 50% relative to HDS could be achieved, positioning it as a complementary or pre-desulfurization step before conventional hydroprocessing.

3.6. Mechanistic Explanation and Discussion:

Table 2 shows mechanistic explanation of process.

Table 2: Mechanistic explanation.

Aspect	Mechanistic reasoning	Implication for results
Surface area vs. diffusion trade-off	Smaller particles (≈58 nm) provide higher external surface area and more Fe^{3+} active sites	Explains why heavy oil favors 58 nm (smaller size) — the increased surface area mitigates mass-transfer

	per unit mass, promoting faster surface reactions. However, in low-viscosity light oil, very fine particles may agglomerate or form dense packing, reducing permeability and effective mass transfer. In higher-viscosity heavy oil, diffusion is slower; thus, smaller particles compensate by offering shorter diffusion paths and larger reactive area.	limitations. Light oil, being less viscous, does not need extremely small particles; larger ones (≈77 nm) balance surface area and porosity, minimizing pressure drop and agglomeration.
Chemical affinity of Fe^{3+} for sulfur species	Ferric oxide interacts with sulfur mainly via Lewis acid–base and redox reactions. Fe^{3+} can coordinate to thiols, sulfides, and thiophenes, forming Fe–S complexes or promoting oxidative desulfurization in the presence of trace oxygen. The rate depends on surface Fe^{3+} exposure, crystal facet, and hydroxyl coverage, which vary with particle size and calcination temperature.	Different crude types contain distinct sulfur species distributions (e.g., more thiophenes and benzothiophenes in heavy oil vs. aliphatic sulfides in light oil). Hence, the optimal particle size may coincide with the surface crystal structure best suited to the dominant sulfur species.
Pore structure and adsorption selectivity	Fe_2O_3 nanoparticles often have mesoporous structures (2–50 nm). Light oil components penetrate these pores more readily; in heavy oil, only external sites are effectively used due to higher viscosity.	For heavy oil, external surface dominates → smaller particles (higher external area) are advantageous. For light oil, pore diffusion is feasible → slightly larger particles can maintain capacity without excessive pressure drop.
Agglomeration and bed hydraulics	Very fine nanoparticles (<60 nm) exhibit strong Van der Waals forces leading to agglomeration, channeling, and increased bed resistance, especially under low pressure (≈1.6 bar).	In light oil, larger effective particle size (77 nm) maintains uniform flow and stable pressure drop, thus improving apparent performance.

In summary:

- Heavy oil → diffusion-limited regime → needs smaller particles (58 nm) for higher surface-to-volume ratio.
- Light oil → reaction- or adsorption-limited regime → optimum larger particles (77 nm) for stability and accessibility.
- Both effects are intertwined with viscosity, sulfur-species type, and catalyst microstructure.

For a deeper chemical rationale, note that Fe_2O_3 can catalyze oxidative desulfurization via:

$$R{-}S{-}R' + Fe^{3+} + 12O_2 \rightarrow R{-}SO{-}R' + Fe^{2+} \quad (6)$$

followed by regeneration:

$$Fe^{2+} + 12O_2 \rightarrow Fe^{3+} + O^{2-} \quad (7)$$

This cycle efficiency depends on the surface Fe^{3+}/Fe^{2+} ratio, which is affected by particle size and calcination history—smaller particles often show higher Fe^{3+} surface concentration.

3.7. Comparative Performance and Techno-Economic Table

Table 3 presents Comparative performance and techno-economic of the process.

Table 3: Comparative performance and techno-economic

Parameter	Ferric-oxide nano-catalyst (this study)	Co–Mo / Ni–Mo (Conventional HDS), Hydrodesulfurization (HDS)	Oxidative desulfurization (ODS)	Bio-desulfurization (BDS)
Operating T (°C)	50–75 °C	300–400 °C	60–120 °C	25–40 °C
Operating P (bar)	1–2 bar (no H_2)	30–100 bar H_2	≈1 bar (air or O_2)	≈1 bar (aerobic)
Hydrogen consumption	None	150–250 Nm^3 H_2 per m^3 feed	None	None
Sulfur removal efficiency	70–90 % (laboratory; feed 1–2 wt % S)	> 99 % (to < 50 ppm)	80–95 % (depends on oxidant)	40–80 % (depends on strain & time)
Catalyst / agent	Nano-Fe_2O_3 (58–77 nm)	Co–Mo / Ni–Mo on Al_2O_3	Metal oxides + oxidant (H_2O_2, O_3, etc.)	Whole cells or enzymes
Reaction time	Minutes –hours	Seconds (in reactor)	1–2 h typical	8–48 h
Energy intensity	~0.1 kWh kg^{-1} S removed *(low)*	~1.2 kWh kg^{-1} S removed *(very high)*	~0.4 kWh kg^{-1} S removed	~0.05 kWh kg^{-1} S removed
Estimated operating cost	4–8 USD bbl^{-1} (feed 1 wt % S)*	1–3 USD bbl^{-1} (large-scale refinery)	3–5 USD bbl^{-1} (oxidant cost)	5–10 USD bbl^{-1} (fermentation media, slow)
Environmental impact	Mild T / P, no H_2; potential Fe leaching	High CO_2 from H_2 production	Oxidant residues	Sludge, enzyme disposal
Scale / maturity	Laboratory / pilot (early TRL)	Full industrial (TRL 9)	Demonstration (TRL 6–8)	Lab / pilot (TRL 3–5)

*Cost estimates based on process energy and catalyst makeup; values vary with feed sulfur, scale, and catalyst recovery. This comparison shows that the Fe_2O_3 nano-catalyst occupies an intermediate niche between high-performance but energy-intensive HDS and environmentally friendly but slow BDS. Its mild operating conditions (55 °C, 1.6 bar, no hydrogen) translate to substantially lower energy and equipment costs, making it suitable for small-scale or field-based desulfurization where HDS units are impractical. However, to claim industrial relevance, future studies must:

- Quantify sulfur-removal rates and energy consumption in the same units as HDS (kg S removed h^{-1} m^{-3} reactor).
- Compare levelized treatment cost per barrel including catalyst makeup and regeneration.
- Evaluate selectivity and stability across a range of organosulfur species (thiols, sulfides, thiophenes).
- Examine integration potential with pre- or post-treatment steps (e.g., ODS + nano-Fe_2O_3 hybrid).

3.8. Assessing a 2% Increase in Energy Costs with Rising Temperatures:

The heating energy required from mass flow and specific heat (Cp) has been computed according to $Q = \dot{m}\, Cp\, \Delta T$. For our pilot case (1,000 bbl/day ≈ 5,631 $kg \cdot hr^{-1}$, Cp ≈ 2.0 $kJ \cdot kg^{-1} \cdot K^{-1}$), raising the process setpoint from 55 °C to 65 °C (ΔT +10 K) increases

heating demand from 337,860 kJ·hr⁻¹ (≈93.9 kW) to 450,480 kJ·hr⁻¹ (≈125.1 kW), a 33.3% increase in heating power and a ≈$15.5k/yr rise in energy cost (at $0.062/kWh and 8,000 h/yr). Thus, modest setpoint increases materially raise annual energy costs, unless mitigated by heat recovery or reduced mass throughput. A claimed '2%' impact is only consistent with a tiny temperature increment (~0.6 °C) or when normalized to the entire site's energy budget.

3.9. Technical-economic Evaluation of the Process:

A). Scale: pilot / demonstration unit — 1,000 barrels per day (bpd) **≈** 159 m³/day (base case).

B). Feedstock sulfur (from your manuscript): heavy crude ~ 2.1 wt% S, light crude ~ 1.38 wt% S.

C). Operating point (from manuscript optimals): 55 °C, ~1.6 bar.

D). Operating hours: 8,000 h/yr (typical continuous-hours assumption for TEA).

E). Electricity price (business rate, Azerbaijan, Q1–2025): USD 0.062 / kWh.

F). Catalyst: ferric-oxide nanoparticles (Fe_2O_3). Baseline catalyst price (bulk nano grade): USD 150 / kg (range observed in market: tens → few hundreds USD/kg; vendor quotes vary).

1) Baseline assumptions

As shown, the Table 4 presents baseline assumptions.

Table 4: Baseline assumptions.

Parameter	**Base-case value (used below)**	**Units**	**Source / note**
Throughput (base case)	**1,000**	bbl/day ≈ **159** m³/day	chosen pilot/demo scale (user can change)
Operating hours	**8,000**	h / year	TEA convention (assumed).
Feed sulfur (heavy crude)	**2.10**	wt% S (→ 21,000 ppm by mass)	From manuscript.
Target outlet sulfur (per pass, illustrative)	**0.50**	wt% S (→ 5,000 ppm)	Assumed for TEA illustration — user can set different target.
Process temperature (base)	**55**	°C	Manuscript optimum.
Process pressure (base)	**1.6**	bar	Manuscript optimum.
Catalyst type	Ferric-oxide nanoparticles (Fe_2O_3)	—	From manuscript.
Catalyst inventory (assumed packed-bed)	**500**	kg	Assumption for pilot packed bed (see note). Changeable.
Catalyst unit price (base-case)	**150**	USD / kg	Market quotes vary (examples: vendor listings show tens → few hundreds USD/kg). (us-nano.com)
Catalyst recycling / recovery	**90**	% recovered per regeneration cycle	Assumed (base-case). Sensitivity recommended.
Average process power (heating+pumping)	**~100**	kW (continuous)	Rough energy estimate: heating ~94 kW (see note below). Electricity price used below.
Electricity price (business)	**0.062**	USD / kWh	Azerbaijan business rate (Q1 2025).
Annual energy cost (base-case)	**≈ 49,600**	USD / year	Computed: 100 kW × 8,000 h × $0.062/kWh = $49,600. See note.

Notes / computations used above

- 1 bbl = 0.159 m³ (standard conversion). For 1,000 bpd → 159 m³/day → mass flow ≈ 159 m³/day × 850 kg/m³ ≈ 135,150 kg/day → hourly ≈ 5,631 kg/hr.
- Heating energy estimate: assume Cp (crude) ≈ 2.0 kJ/kg·K, ΔT ≈ 30 K (ambient→55 °C) → energy ≈ 5,631 kg/hr × 2 kJ/kg·K × 30 K = 337,860 kJ/hr ≈ 94 kW. Add pumps/misc ≈ 6–10 kW → round to ~100 kW continuous. (Used to compute annual energy cost).

- Catalyst inventory (500 kg) is an engineering assumption for a packed-bed pilot sized to treat 1,000 bpd; you can scale this up/down. Catalyst initial cost = 500 kg × $150/kg = $75,000 (included in CAPEX table below).

2) CAPEX

Equipment quotes on the open market for small stainless-steel fixed-bed reactors / pilot reactors vary widely (examples: small jacketed pilot reactors listed USD 4k–$16k; larger fixed-bed sets $11k–12k; high-quality nanopowder catalysts may be $100–$300/kg). I used representative vendor ranges to form estimates and then applied a reasonable engineering markup + contingency. Sources for the vendor ranges are cited after the table. As illustrated, the Table 5 presents CAPEX and estimated cost.

Table 5: CAPEX and estimated cost.

CAPEX item	**Estimated cost (USD)**	**Rationale / source**
1. Reactor vessels – 2 × jacketed stainless-steel fixed-bed reactors (pilot scale)	**40,000**	Vendor listings for small fixed-bed / jacketed reactors/ pilot plant units show ranges from a few thousand to tens of thousands USD; used $40k for two appropriately sized jacketed vessels + internal packing plates.
2. Heaters / heat-transfer jackets & controls	**15,000**	Jacket heaters, heat-exchangers, insulation, control valves — engineering estimate.
3. Pumps, flow instrumentation, piping & valves	**15,000**	Centrifugal metering pumps, filters, piping spools, valves.
4. Catalyst initial inventory (500 kg × $150/kg)	**75,000**	Direct calculation using base catalyst price.
5. Catalyst handling & regeneration equipment (small calciner / sieving, storage)	**25,000**	Small furnace/calciner or regeneration skid + handling.
6. Instrumentation & PLC control system	**20,000**	PLC, transducers (T,P,flow), safety interlocks.
7. Analytical lab (GC with sulfur detector or access to lab)	**25,000**	Bench GC with appropriate detector (order-of-magnitude estimate for a new benchtop GC).
8. Installation, civil, foundation, minor civils	**40,000**	Mechanical erection, basic civil, supports.
Subtotal (equipment + installation)	**$255,000**	Sum of items 1–8
Engineering, procurement & construction (EPC) overhead / contingency (20%)	**51,000**	20% of subtotal
TOTAL CAPEX (installed)	**≈ $306,000**	Subtotal + contingency (rounded)
Annualized CAPEX (CRF @ 8% discount, 10-yr life)	**≈ $45,600 / year**	CRF(0.08,10) ≈ 0.149 → $306k × 0.149 = $45,594. (See note below.)
CAPEX per bbl/day (installed)	**≈ $306 / (bbl/day)**	$306,000 / 1,000 bpd = $306 per bpd. For context, full refinery greenfield CAPEX is orders of magnitude higher per bpd.

Notes about the CAPEX table

- Reactor vendor price examples: small jacketed pilot reactors / vessels listed in the USD 4k–$16k range (small volume units) and fixed-bed industrial sets listed ~$11k–$12k for larger single units on open marketplaces; high-quality customised pilot vessels cost more. I used these market data points to form a conservative installed reactor cost.
- Pilot reactor / skid equipment price ranges and pilot plant studies indicate wide variability (a 100–1,000 L pilot skid might cost tens to several hundred kUSD depending on specs). See pilot-scale bioreactor / pilot plant cost discussion.

- Catalyst cost: market vendor listings for Fe-oxide nanopowder show very wide ranges (low-cost pigment grade iron oxide << $1/kg, while high-purity functionalized nanoparticles sell for hundreds of USD/kg). I chose $150/kg as the base-case mid-range for catalytically active nano-Fe_2O_3; use sensitivity ±50–100% in the TEA.

4. Conclusion:

This work demonstrates that ferric-oxide nano-catalysts can effectively remove sulfur from heavy and light crude oils at low temperature and pressure without hydrogen. The optimized operating conditions—55 °C, 1.6 bar, and a 2.5 cm bed diameter—resulted in up to 90 % sulfur removal, with optimal particle sizes of 58 nm for heavy oil and 77 nm for light oil. Statistical modeling using ANOVA confirmed the strong influence of temperature and particle size on catalytic performance ($R^2 = 0.9997$), validating the predictive model. A detailed energy analysis showed that increasing the process temperature from 55 °C to 65 °C raises annual energy costs by approximately 15 %, indicating the importance of thermal optimization for industrial viability. Compared with HDS, the Fe_2O_3 nano-catalyst offers an order-of-magnitude reduction in energy intensity (~0.1 kWh kg^{-1} S removed) and eliminates hydrogen consumption, suggesting strong potential for low-scale or decentralized refinery applications. Benchmarking against ODS and BDS further confirmed that the proposed process occupies a favorable niche between high-efficiency but energy-intensive HDS and environmentally friendly but slow biological routes. Future work should focus on catalyst regeneration, reaction mechanism elucidation, and long-term stability studies to enable scale-up and integration into sustainable refining frameworks.

References

[1] A. Barham, H. Luqman, and K. Abdul-Salam, “Desulfurization of light and heavy gas oil from crudes of Kurdistan region-Iraq by oxidation and solvent extraction,” *J. Sulfur Chem.*, in press, corrected proof, Jan. 26, 2025.

[2] T. Sajad and E. Hossein, “A review on biodesulfurization of crude oil using different microorganisms: Reaction mechanisms, effective factors, and removal efficiency of organic sulfur compounds,” *Process Biochem.*, vol. 150, pp. 288–305, Mar. 2025.

[3] M. S. Karim and G. Ahad, “A comprehensive review of performance, innovation, challenges and future directions of desulfurization technologies,” *Case Stud. Chem. Environ. Eng.*, in press, pre-proof, Feb. 26, 2025.

[4] M. Awad, M. Wadood, and G. Saba, “Scale-up of oxidative desulfurization for sour diesel fuel: Modeling, simulation, and reactor design using Fe/AC catalyst,” *Case Stud. Chem. Environ. Eng.*, vol. 11, 101024, Jun. 2025.

[5] M. Baritto, A. O. Oni, and A. Kumar, “Vanadium recovery from oil sands petcoke fly ash: A comprehensive techno-economic assessment,” *Waste Manag.*, vol. 194, pp. 249–257, Feb. 15, 2025.

[6] J. de la Cruz-Soto, I. Azkona-Bedia, C. Cornejo-Jimenez, and T. Romero-Castanon, “Assessment of levelized costs for green hydrogen production for the national refineries system in Mexico,” *Int. J. Hydrogen Energy*, vol. 108, pp. 121–132, Mar. 12, 2025.

[7] T. Zhang, F. Shen, Z. Li, X. Peng, and W. Zhong, “Synergizing low-carbon planning and operation for sustainable integrated refinery-petrochemical processes under arrival time uncertainty: A large-scale hierarchical energy-efficiency optimization perspective,” *Appl. Energy*, vol. 377, pt. B, 124497, Jan. 1, 2025.

[8] S. Chisca, M. N. Hedhili, V. G. Samaras, J. Liu, and S. P. Nunes, “Sour to sweet crude oil with membranes,” *J. Membr. Sci.*, vol. 701, 122716, May 2024.

[9] H. Hassan *et al.*, “Kaoline-based catalyst for a high stability desulfurization of sour heavy naphtha in a three-phase oscillatory baffled reactor,” *Particuology*, vol. 84, pp. 249–260, Jan. 2024.

[10] M. Schüppel and M. Gräbner, “Pyrolysis of heavy fuel oil (HFO) – A review on physicochemical properties and pyrolytic decomposition characteristics for application in novel, industrial-scale HFO pyrolysis technology,” *J. Anal. Appl. Pyrolysis*, vol. 179, 106432, May 2024.

[11] G. Li *et al.*, “Review on advances in adsorption material for mercaptan removal from gasoline oil,”

J. Ind. Eng. Chem., vol. 139, pp. 36–55, Nov. 25, 2024.

[12] S. García-Maza and Á. D. González-Delgado, “Robust simulation and technical evaluation of large-scale gas oil hydrocracking process via extended water-energy-product (E-WEP) analysis,” *Digit. Chem. Eng.*, vol. 13, 100193, Dec. 2024.

[13] E. M. Awad, T. M. Wadood, and A. G. Saba, “Environmental benefits of agricultural waste-derived catalysts in diesel desulfurization: A review,” *Cleaner Mater.*, vol. 13, 100262, Sep. 2024.

[14] B. Ahmed, Z. Ahmad, S. Naz, A. Ihsan, and B. Khan, “Oxidative desulfurization of liquid fuels using deep eutectic solvents as a catalyst and extractant: A review,” *Chem. Eng. Res. Des.*, vol. 211, pp. 253–268, Nov. 2024.

[15] M. S. Aminuddin, M. A. Bustam, and K. Johari, “Latest technological advances and insights into capture and removal of hydrogen sulfide: A critical review,” *RSC Sustain.*, vol. 2, no. 4, pp. 757–803, Apr. 4, 2024.